Observation of the reversible ice III to ice IX phase transition by using ammonium fluoride as anti-ice II agent

Christoph G. Salzmann,[a] Zainab Sharif,[a] Ben Slater,[a] Craig L. Bull,[b] Martin Hart[a]*

[a] Department of Chemistry, University College London, 20 Gordon Street, London WC1H 0AJ, United Kingdom; email: c.salzmann@ucl.ac.uk

[b] ISIS Pulsed Neutron and Muon Source, Rutherford Appleton Laboratory, Harwell Oxford, Didcot OX11 0QX, United Kingdrom.

ABSTRACT

Ice III is a hydrogen-disordered phase of ice that is stable between about 0.2 and 0.35 GPa. Upon cooling, it transforms to its hydrogen-ordered counterpart ice IX within the stability region of ice II. Because of this metastability, detailed studies of the ice III to ice IX phase transition have so far not been carried out. Using ammonium fluoride doping to prevent the formation of ice II, we now present a detailed study on this phase transition using in-situ powder neutron diffraction. The *a* and *c* lattice constants are found to expand and contract, respectively, upon hydrogen ordering yielding an overall negative volume change. Interestingly, the anisotropy in the lattice constants persists when ice IX is fully formed and negative thermal expansion is observed. Analogous to the isostructural keatite and *β*-spodumenes, the negative thermal expansion can be explained through the build-up of torsional strain within in the *a*-*b* plane as the helical 'springs' within the structure expand upon heating. The reversibility of the phase transition was demonstrated for the first time upon heating. The ammonium fluoride doping induces additional residual hydrogen disorder in ice IX and is suggested to be a chemical way for 'excitation' of the ice-rules configurational manifold. Compared to ices II and VIII, the induced hydrogen disorder in ice IX is smaller which suggests a higher density of configurational states close to the ground state. This study highlights the importance of dopants for exploring water's phase diagram and underpins the highly complex solid-state chemistry of ice.

INTRODUCTION

Ice III occupies the smallest region of thermodynamic stability in the phase diagram of H_2O.[1, 2] As shown in Figure 1(a), it is stable between about 0.2 and 0.35 GPa, and over a temperature range of ~10 K sharing triple points with the 'ordinary' ice I*h*, ice II, ice V and liquid water.[3-5] Since ice III forms at quite moderate pressures, it is believed to be part of the ice shells of several of the icy moons in the Solar system.[6-8] Its hydrogen-bonded network of water molecules is isostructural with the keatite silica polymorph and described by the tetragonal $P4_12_12$ space group.[9-13] This makes ice III a chiral phase of ice[1] together with the recently discovered ice XVII.[14] The unit cells of ice III using the $P4_12_12$ space group and its enantiomorphic counterpart $P4_32_12$ are shown in Figure 1(b). The structures contain two crystallographically distinct oxygen sites and three different types of hydrogen bonds. A defining structural feature are four-fold spirals along the crystallographic *c* axis, which, depending on the space group, display a different handedness. The spirals contain one type of hydrogen bond whereas the other two arise from water molecules hydrogen bonding to four neighboring spirals.[9-12]

Originally, the hydrogen-bonded water molecules in ice III were believed to be fully orientationally disordered.[15, 16] In diffraction, such a fully hydrogen-disordered structure can be described with half-occupied hydrogen sites reflecting the average structure. However, in-situ neutron diffraction of ice III in its region stability has shown that the fractional occupancies of the six crystallographically distinct deuterium sites deviate from ½.[17-19] Considering the ice rules, the six occupancies can be described with two order parameters α and β that range from 0 to 1 and hence define the extent of hydrogen (dis)order of the hydrogen bonds between and within the four-fold spirals, respectively.[12] At 250 K and 0.3

GPa, α and β were found to take values of 0.36 and 0.53.[19] The small deviations from 0.5 mean that ice III is classified as a partially ordered hydrogen-disordered phase of ice.

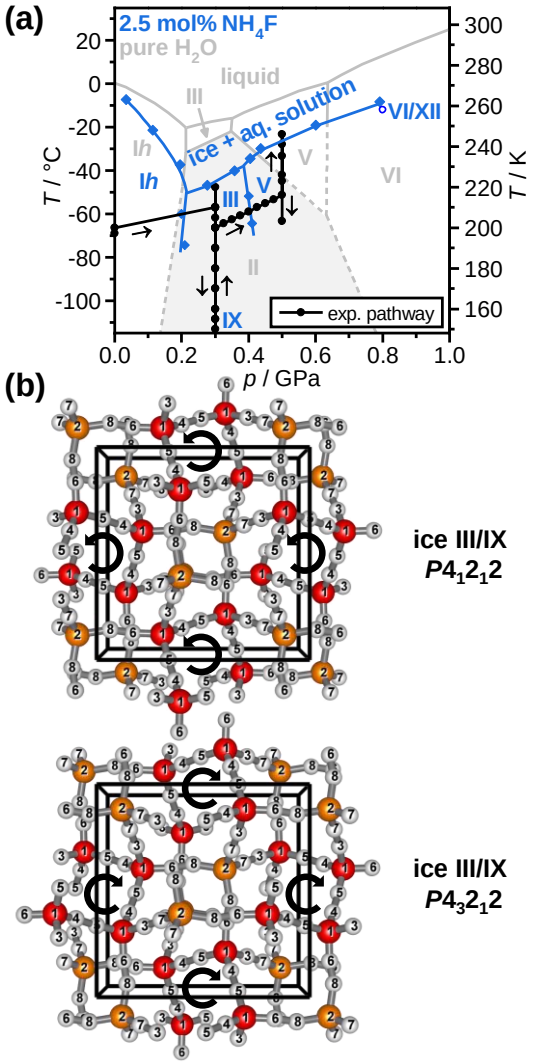

Figure 1. *(a) Phase diagram of pure ice (gray) and ice with 2.5 mol% NH_4F (blue).[20] The experimental pathway using 2.5 mol% ND_4F in this study is indicated by full black circles. (b) Unit cell of ice III/IX using the $P4_12_12$ spacegroup (top) as well as the corresponding enantiomorphic space group $P4_32_12$ (bottom). The crystallographically distinct oxygen sites are shown as red and orange spheres, and the hydrogen sites as smaller white spheres. The labelling of the atoms is as defined in ref. [12]. The circular arrows indicate the handedness of the 4-fold screw axes.*

Upon cooling under pressure, ice III transforms to its antiferroelectric hydrogen-ordered counterpart ice IX between 208 and 165 K.[21] In Kurt Vonnegut's novel Cat's Cradle, 'ice-nine' is a fictional deadly form of ice that stable at ambient conditions.[22] In stark contrast to this, the real ice IX is always metastable with respect to ice II at temperatures below the region of stability of ice III.[23] Due to its metastability, ice IX is often found in sequences of phase transitions at low temperatures following Ostwald's rule of stages up to ~0.7 GPa.[24, 25] Using single-crystal neutron diffraction, it was shown that D_2O ice IX contains a small amount of residual hydrogen disorder ($\alpha = 0.034$ and $\beta = 0.051$).[12, 17] The ice III to ice IX phase transition is the only hydrogen-ordering phase transition in ice observed so far where the space group symmetry does not change.[9-12, 17, 26-29] Using DFT calculations, the experimental structure of ice IX was shown to display the lowest energy out of the four possible ordered arrangements in $P4_12_11$.[30]

The phase transition from ice III to ice IX upon cooling under pressure was followed with dielectric spectroscopy,[21] calorimetry[31] and Raman spectroscopy.[32] It was found that cooling rates greater than 1-2 K min^{-1} are needed in order to suppress the transformation to the stable ice II.[32, 33] The irreversible transformation to ice II has therefore prevented in-situ neutron diffraction studies of the ice III to ice IX phase transition so far,[17, 33] which require long measurement times. Upon heating, ice XI always transforms to the stable ice II[21, 31, 32] which means that it was not possible so far to demonstrate the reversibility of the ice III / IX phase transition.

Recently, we have shown that the fully hydrogen-ordered ice II can be selectively destabilized using small amounts of ammonium fluoride (NH_4F) doping so that ice III becomes the stable phase at 0.3 GPa.[20] The mechanism for this is that NH_4F acts as a hydrogen disordering agent which has also recently been demonstrated for the ice VII to ice

VIII phase transition.[34] Since ice III is already hydrogen-disordered, its free energy is not significantly affected by the NH_4F dopant.

Here we make use of the anti-ice II effect of NH_4F to study the ice III / IX phase transition with in-situ powder neutron diffraction. The changes in lattice constants and unit-cell volume upon hydrogen (dis)ordering are determined and discussed in the context of recent studies of other hydrogen (dis)ordering phase transitions,[35-39] and the hydrogen-disordering effect of NH_4F on ices III and IX is investigated. Furthermore, the experimental changes in the lattice constants are compared with computational calculations.

EXPERIMENTAL AND COMPUTATIONAL METHODS

Deuterated ammonium fluoride (ND_4F) was obtained by dissolving NH_4F (99.99% trace metal basis) in an excess of deuterated water (99.9% D) followed by complete evaporation of the liquid by boiling under a constant flow of dry nitrogen gas. To ensure complete deuteration, the dissolution in D_2O followed by evaporation was repeated twice. The resulting dry ND_4F powder was stored in a desiccator and used to prepare a 2.5 mol% solution in D_2O. Complete deuteration was confirmed from the absence of N–H stretching modes in Raman spectroscopy. All ND_4F solutions were prepared and handled in polyethylene containers.

A few milliliters of the 2.5 mol% solution was frozen in a porcelain pestle and mortar precooled with liquid nitrogen. After grinding for a few minutes, the fine powder was transferred into a cylindrical TiZr cell with a Bridgman seal at the bottom which was attached to a gas-intensifier unit while keeping the pressure cell cold with external dry ice. Argon gas was used as a pressure medium. To create a seal, the pressure was quickly increased to 1500 bar and then released again. For temperature measurements, a thermocouple was attached to the TiZr cell with a copper ring. The gas-cell was then mounted onto a cryostat stick and

lowered into a helium cryostat precooled to 200 K on the PEARL beamline at ISIS.[40] The temperature / pressure pathways of the experiment are shown in Figure 1(a). For ices III/IX, two long runs were recorded at 210 K and 150 K for 1500 μA hours of proton current (~9 h) while shorter runs of 150 μA h (~ 1h) were recorded at the other temperatures. All neutron diffraction patterns were collected at 90° scattering angle and analyzed using the GSAS software.[41] The ice IX structure from ref. [12] was generally found to be the best starting structure for the refinements.

All density functional theory calculations were performed with the quickstep module of the CP2K code[42] using the PBE functional and van der Waals corrections were implemented through the Grimme D3 scheme.[43] Double zeta "MOLOPT" basis sets were used in conjunction with a 1200Ry cutoff. All cell relaxations were performed without any constraints on the symmetry or the cell parameters. For the four possible configurations of ice IX we used 2×2×2 supercells. Direct cell optimizations were performed with simultaneous update of coordinates and cell parameters.

RESULTS AND DISCUSSION

As shown in Figure 2(a), the experiment started with the compression of the 2.5 mol% ND_4F doped sample from ambient pressure to 0.3 GPa while increasing the temperature to 210 K. In line with our previous experiments, the compression resulted in the transformation of ice I*h* to ice III and a small amount of the cubic structure II argon clathrate hydrate due to the pressure medium (see Figure 2(b,c)).[20] To probe the formation of ice IX, the sample was then cooled to 150 K while keeping the pressure constant at 0.300 GPa. This was achieved over a period of ~ 12 hours while recording powder patterns at least every 10 K. To emphasize this point, such a cooling procedure would inevitably result in the formation of ice

II in the case of pure ice since the cooling rate was considerably lower than the 1-2 K min^{-1} needed to suppress the formation of ice II.[32, 33]

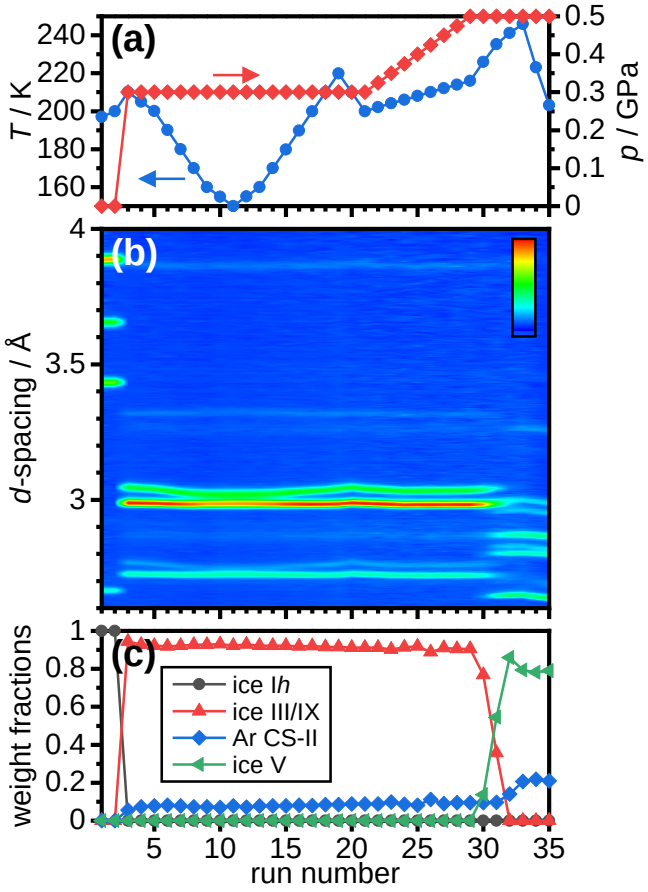

Figure 2. *(a) Changes in temperature and pressure during the experiment. (b) Neutron diffraction patterns of the D_2O plus 2.5 mol% ND_4F sample displayed as a contour plot. A color scale bar is shown in the top right-hand corner. (c) Changes in weight fractions of ice Ih, ice III/IX, cubic structure II argon clathrate hydrate and ice V as the experiment progresses.*

The formation of ice IX upon cooling can be seen clearly from the merging of the 102 and 201 Bragg peaks around 3 Å as the tetragonal ice III transforms into ice IX which is close to pseudo-cubic.[9-12] A similar merging of peaks is also seen for the weaker 112 and 211 Bragg peaks just above 2.7 Å. The reversibility of the phase transition is demonstrated upon

heating to 220 K when the two groups of peaks split again. While the ice III to ice IX phase transition has been previously observed using other methods and fast cooling rates, the reverse ice IX to ice III phase transition has so far not been observed since pure ice IX always transforms to ice II upon isobaric heating.[21, 31, 32]

The changes in lattice constants and unit-cell volume upon cooling ice III from 210 K are shown as blue diamonds in Figure 3. The *a* lattice constant changes very little initially and then begins to increase below 200 K. This change in slope seems to indicate the onset of the phase transition from ice III to ice IX. Interestingly, it is difficult to spot an endpoint of the phase transition as the *a* lattice constant continues to increase upon cooling below 160 K. In the case of pure ice III, the *a* lattice constants has been shown to contract between 250 and 240 K at 0.25 GPa.[19] In ref. [20], we heated a 2.5 mol% ND_4F sample from 200 to 250 K. Due to the incongruent melting, only the lattice constants up to 225 K were included as gray squares in Figure 2. Upon partial melting, the ND_4F may be enrich in the liquid phase thereby changing the composition of the solid ice phase. This would be problematic since the amount of dissolved ND_4F affects the lattice constants of ice slightly.[20, 44, 45] For the *a* lattice constant, a minimum is observed in this data at 215 K. All in all, the *a* lattice constant appears to contract at first upon cooling ice III from its region of stability followed by a plateau and then an expansion as the sample undergoes the phase transition to ice IX. This expansion seems to continue upon cooling even once ice IX has fully formed.

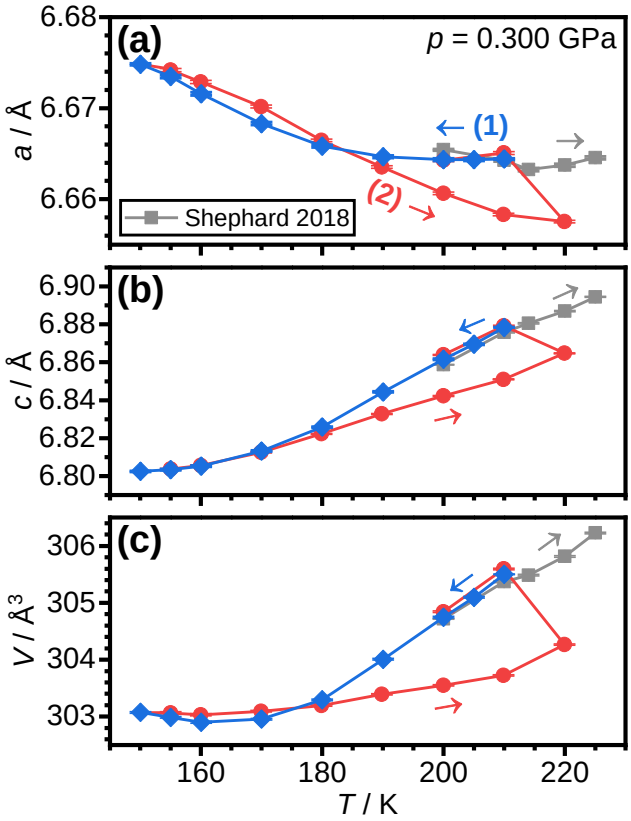

Figure 3. Lattice constants and unit-cell volume of D_2O ice III/IX with 2.5 mol% ND_4F recorded upon cooling from 210 K (blue diamonds) and subsequent heating at 0.3 GPa (red circles). Data points obtained upon heating from 200 K (gray squares) are from ref. [34].

The *c* lattice constant contracted as pure ice III is cooled from 250 to 240 K at 0.25 GPa.[19] From the data shown in Figure 3(b), it can be seen that *c* contracts at all temperatures as our sample was cooled. The most pronounced changes in *c* are observed during the ice III to ice IX phase transition in the 200 to 160 K temperature range.

The volume changes of the unit cell in Figure 3(c) show decreases as ice III is cooled and during the phase transition to ice IX. Interestingly, below 160 K, the volume increases upon cooling to 150 K which is caused by the expansion in *a*. Anisotropic thermal expansion and overall negative thermal expansion have also been observed for the isostructural keatite[13] and some related *β*-spodumenes ($Li_2O{\cdot}Al_2O_3{\cdot}nSiO_2$).[46] The contraction of the

a-*b* plane upon heating has be explained by the formation of torsional stress as the helical springs within these materials expand upon heating. It seems as if a similar phenomenon is at play in ice IX as well at low temperatures and 0.3 GPa. Negative thermal expansion has also been observed for the 'ordinary' ice I*h*.[47, 48] However, compared to ice IX, this was observed below 73 K[47] or 60 K,[48] and it did not go along with anisotropic behavior of the lattice constants. Unfortunately, it was not possible to cool ice IX further at 0.3 GPa because the freezing point of argon would have been reached which would have resulted in the loss of pressure. Also, helium or neon could not have been used as the pressure media since they are known to stabilize the ice II structure by intercalation.[49-52]

Heating of the ice IX sample shows some remarkable hysteresis effects. Both the *a* and the *c* lattice constant 'overshoot' the phase transition back to ice III upon heating to 220 K as shown in Figure 3. In fact, only upon cooling to 210 K from 220 K was equilibrium established and the lattice constants agreed with those of the ice III measured before the cooling at both 210 and 200 K. The sluggish hydrogen disordering kinetics could be a general feature of the ice IX to ice III phase transition. However, at least some of this effect is probably due to the ND_4F doping which has previously been shown to slow-down the hydrogen ordering kinetics of the ice VII to ice VIII phase transition.[34] Hydrogen-(dis)ordering phase transitions require the collective reorientation of water molecules along travelling defect pathways within the crystal.[25] The incorporation of ND_4^+ and F^- point defects is thought to terminate such defect pathways which then overall slows down hydrogen (dis)ordering processes.

The effect of ND_4F doping on the extent of hydrogen (dis)order of ice III at 210 K and of ice IX at 150 K was investigated in a next step. Figure 4 shows the Rietveld fits to the diffraction data at these two temperatures. For ice III at 210 K, the two order parameters were

refined as $\alpha = 0.456$ and $\beta = 0.454$. Previously, for pure ice III, these values were determined as 0.36 and 0.53, respectively, at 250 K and 0.3 GPa.[19] The extent of partial order observed in ND_4F doped ice III at 210 K therefore seems to be the consequence of the disordering effect of ND_4F doping on the α parameter and partial ordering due to the lower temperature for β. In any case, both order parameters are slightly below 0.5 which is already the correct trend with respect to the hydrogen ordering towards ice IX at lower temperatures.

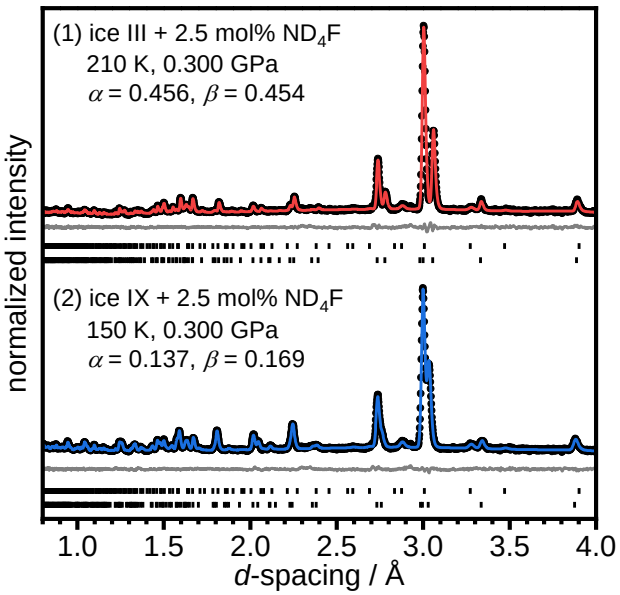

Figure 4. *Rietveld analysis of (1) ND_4F-doped ice III at 210 K and 0.3 GPa and (2) ND_4F-doped ice IX at 150 K and 0.3 GPa. The experimental data are shown as black circles, red or blue lines are the Rietveld fits, and gray lines are the differences between the experimental data and the Rietveld fits downshifted for clarity. The tick marks under each diffraction pattern are for ice III/IX (bottom) and cubic structure II argon clathrate hydrate[53] (top).*

The ND_4F-doped ice IX at 150 K displays $\alpha = 0.137$ and $\beta = 0.169$. For pure D_2O ice IX, α and β were determined as 0.034 and 0.051, respectively, highlighting a small degree of residual hydrogen disorder in ice IX.[12] This illustrates that the ND_4F doping is capable of inducing hydrogen disorder within ice IX as it has been previously observed for ice VIII.[34]

But also, it is important to point out that the way ice IX becomes hydrogen ordered is not changed by the ND_4F dopant. In principle, either one or both of the order parameters could tend towards one instead of zero and thereby form a different hydrogen-ordered structure. Also, as previously observed for pure ice IX, $\alpha < \beta$ for the ND_4F-doped sample indicating that the hydrogen sites that are more disordered in pure ice IX are also more disordered in the ND_4F-doped sample. The complete crystallographic information of the ND_4F-doped ice IX is given in Table 1.

In the case of fully hydrogen-ordered ice VIII, doping with 2.5 mol% ND_4F changed the single order parameter from 0 to 0.156.[34] As mentioned above, for ice IX, the changes using the same amount of ND_4F doping are 0.034 → 0.137 and 0.051 → 0.169 which correspond to changes of 0.103 and 0.118, respectively. The hydrogen-disordering effect of 2.5 mol% ND_4F is therefore slightly less in ice IX than it was for the fully hydrogen-ordered ice VIII. For the fully hydrogen-ordered ice II, the disordering effect of ND_4F was to such an extent that it led to its complete destabilization.[20]

The presence of residual hydrogen disorder in ice IX as opposed to ices II and VIII implies a higher density of partially disordered states close to the energetic ground state. This is now nicely illustrated by the ND_4F doping experiments. In a sense, ND_4F doping can be seen as a chemical way to achieve 'excitation' of the configurational ice-rule manifold. Compared to the partially disordered ice IX, the ND_4F doping achieves a greater 'excitation' away from the ground state in the cases of the fully hydrogen-ordered ices II and VIII.

Lattice constants for the four possible hydrogen ordered arrangements of ice IX in $P4_12_12$ were calculated using Density Functional Theory (DFT) both with and without considering van der Waals interactions[43] using the PBE functional.[54, 55] The results are shown in Figure 5 as the ratios of the lattice constants with respect to the averages of all four

configurations. This is thought to provide a measure for how the lattice constants behave relative to the hydrogen-disordered state.

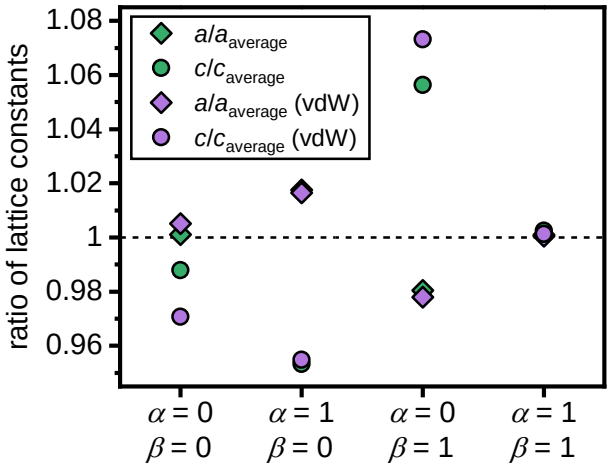

Figure 5. *Ratios of calculated lattice constants of the four possible ice IX configurations with order parameters α and β divided by the averages of all four configurations. The ratios are given with and without considering van der Waals interactions in the calculations.*

The first configuration, with $\alpha = 0$ and $\beta = 0$, corresponds to the experimental configuration found for ice IX both previously and in this study. The DFT calculations predict a small increase in *a* and a more substantial decrease in *c* for the transition from ice III to ice IX. Including van der Waals forces in the calculations makes both changes somewhat larger. For the second configuration ($\alpha = 1$ and $\beta = 0$), the same trends are observed. However, the changes in the lattice constants are more pronounced. Reverse trends with *a* contracting and *c* expanding are predicted for the third configuration ($\alpha = 0$ and $\beta = 1$) which is in clear contradiction with the experimental observations. Finally, the fourth configuration ($\alpha = 1$ and $\beta = 1$) displays weakly positive changes for both lattice constants. From the changes in lattice constants determined in Figure 3, it is difficult to extract accurate values for the hydrogen ordering phase transition since the temperature window of the phase transition is large and

the effects of temperature overlap with those from the ordering transition. Nevertheless, the predicted changes for configurations 3 and 4 are in clear disagreement with the experimental observations. The changes predicted by the second configurations are significantly too large considering the experimental changes. For example, if a *c* value of 6.8 Å is taken for ice IX, this would imply a *c* lattice constant for ice III of about 7.08 Å which is clearly outside the experimentally feasible range. In line with expectation, the predicted changes in the lattice constants of the first configuration are the ones that most closely resemble the experimental ones. Including van der Waals interactions appears to be important for achieving *c*/*a* ratios close to the pseudo-cubic experimental structure of ice IX. The ratios changed from 1.13 to 1.05 upon including van der Waals interactions for the 1st configuration.

The approximate volume change for the ice III to ice IX phase transition is ~–2.5 Å^3 as determined from Figure 3(c). Considering that the unit cell contains 12 water molecules, this gives a molar volume change ΔV of 1.3×10^{-7} m^3 mol^{-1}. Using the negative Pauling entropy (–3.371 Pa m^3 mol^{-1} K^{-1}) as the molar entropy change for this phase transition, gives a Clapeyron slope dT/dp of the ice III / ice IX phase boundary of ~39 K GPa^{-1}. Considering that ice III is partially ordered and ice IX partially disordered, the actual entropy change will be slightly less negative which means that the actual slope is somewhat more positive. According to this, the phase transition temperature from ice III to ice IX is expected to change by about 6 K in the pressure range where ice III is stable. Of course, the ice III to ice IX phase transition does not appear to be a straight-forward first-order phase transition as can be seen from the rather large temperature window in which it takes places. This estimate therefore needs to be treated with caution as different elements of the phase transition could respond differently to pressure.

Nevertheless, it is interesting to note that the volume change for the ice III to ice IX phase transition is negative. This is in contrast to the ice VI to ice XV phase transition for which a positive volume change has been observed upon hydrogen ordering.[36] The positive volume change enable us to suppress hydrogen ordering at pressures greater than ~1 GPa and to isolate so-called 'deep glassy states' of ice VI.[37, 38] Considering the negative volume change of the ice III to ice IX phase transition, obtaining hydrogen-disordered ice III at low temperatures by increasing the pressure seems difficult. However, a way forward could be to increase the ammonium fluoride concentration beyond 2.5 mol% which is expected to slow down the hydrogen kinetics upon cooling. Interesting trends in the lattice constants have also recently been observed for the ice VII to ice VIII phase transition.[39] However, it is at present unclear if the volume change is positive or negative.

In a final step, the ice III sample was compressed to 0.5 GPa while heating from 200 to 246 K as shown in Figure 1(a) and Figure 2. Consistent with our previous piston-cylinder experiments,[20] the phase transition to ice V was observed at about 0.4 GPa. Upon cooling from 246 to 203 K, the ice V persisted as expected since the ND_4F doping prevents the formation of ice II.

CONCLUSIONS

The ice III to ice IX phase transition was followed for the first time with in-situ diffraction by suppressing the phase transition to ice II with small amounts of ammonium fluoride. The hydrogen ordering phase transition in the 200 to 160 K temperature window goes along with an expansion in the *a* lattice constant and contraction in *c* which corresponds to a shrinking of the helical springs in the crystal structure. Overall, the volume decreases during the ice III to ice IX phase transition. Below 160 K, the *a* lattice constants continues to expand which interestingly leads to a volume expansion as the ice IX is cooled. This unusual behavior has

previously been observed for the isostructural keatite and related spodumene materials, and has been attributed to the build-up of torsional strain within the *a*-*b* plane as the helical 'springs' contract.

The reversibility of the ice IX to ice III phase transition upon heating has been demonstrated for the first time including significant hysteresis effects. These may be due to the ND_4F dopant which is known to slow down hydrogen (dis)ordering kinetics. Interestingly, the hydrogen-disordering effect of ND_4F on ice IX was found to be less compared to ice VIII. This led us to propose that doping with ammonium fluoride can be regarded as a chemical way to achieve 'excitation' of the configurational ice-rule manifold. In the case of ice IX, the ND_4F doping indicates a higher density of states close to the ordered ground state compared to, for example, ices II and VIII. It can also now be concluded that all hydrogen-ordered phases of ice that form in the absence of dopants (*i.e.* ices II, IX and VIII) can be hydrogen-disordered with ammonium fluoride doping. These findings underpin once more the highly complex solid-state chemistry of ice.

ACKNOWLEDGMENTS

Funding is acknowledged from the European Research Council under the European Union's Horizon 2020 research and innovation programme (grant agreement No 725271). We thank ISIS for granting access to the PEARL instrument, and we are grateful to C. Ridley (ISIS crystallography group), C. Goodway and M. Kibble (ISIS pressure support) for help with the neutron diffraction experiment. We acknowledge the use of ARCHER via our membership of the UK's HEC Materials Chemistry Consortium, which is funded by EPSRC (EP/L000202, EP/R029431).

DATA AVAILABILITY STATEMENT

Raw data were generated at the ISIS large scale facility. Derived data supporting the findings of this study are available from the corresponding author upon reasonable request. The raw data are available at https://doi.org/10.5286/ISIS.E.86391366.

REFERENCES

[1] C. G. Salzmann, J. Chem. Phys. **150**, 060901 (2019).

[2] M. Millot, F. Coppari, J. R. Rygg, A. Correa Barrios, S. Hamel, D. C. Swift, and J. H. Eggert, Nature **569**, 251 (2019).

[3] G. Tammann, Ann. Phys. **2**, 1 (1900).

[4] P. W. Bridgman, J. Chem. Phys. **5**, 964 (1937).

[5] P. W. Bridgman, Proc. Am. Acad. Arts Sci. **47**, 441 (1912).

[6] K. Echelmeyer, and B. Kamb, Geophys. Res. Lett. **13**, 693 (1986).

[7] F. Sohl, T. Spohn, D. Breuer, and K. Nagel, Icarus **157**, 104 (2002).

[8] W. B. Durham, S. H. Kirby, and L. A. Stern, J. Geophys. Res. **102**, 16293 (1997).

[9] W. B. Kamb, and S. K. Datta, Nature **187**, 140 (1960).

[10] B. Kamb, and A. Prakash, Acta Cryst. **B24**, 1317 (1968).

[11] S. W. Rabideau, E. D. Finch, G. P. Arnold, and A. L. Bowman, J. Chem. Phys. **49**, 25142519 (1968).

[12] S. J. La Placa, and W. C. Hamilton, J. Chem. Phys. **58**, 567 (1973).

[13] P. P. Keat, Science **120**, 328 (1954).

[14] L. del Rosso, F. Grazzi, M. Celli, D. Colognesi, V. Garcia-Sakai, and L. Ulivi, J. Phys. Chem. C **120**, 26955 (2016).

[15] G. J. Wilson, R. K. Chan, D. W. Davidson, and E. Whalley, J. Chem. Phys. **43**, 2384 (1965).

[16] E. Whalley, and D. W. Davidson, J. Chem. Phys. **43**, 2148 (1965).

[17] J. D. Londono, W. F. Kuhs, and J. L. Finney, J. Chem. Phys. **98**, 4878 (1993).

[18] W. F. Kuhs, C. Lobban, and J. L. Finney, Rev. High Pressure Sci. Technol. **7**, 1141 (1998).

[19] C. Lobban, J. L. Finney, and W. F. Kuhs, J. Chem. Phys. **112**, 7169 (2000).

[20] J. J. Shephard, B. Slater, P. Harvey, M. Hart, C. L. Bull, S. T. Bramwell, and C. G. Salzmann, Nat. Phys. **14**, 569 (2018).

[21] E. Whalley, J. B. R. Heath, and D. W. Davidson, J. Chem. Phys. **48**, 2362 (1968).

[22] K. Vonnegut, *Cat's Cradle* (Holt, Rinehart and Winston, New York, USA, 1963),

[23] V. F. Petrenko, and R. W. Whitworth, *Physics of Ice* (Oxford University Press, Oxford, 1999),

[24] C. G. Salzmann, E. Mayer, and A. Hallbrucker, Phys. Chem. Chem. Phys. **6**, 5156 (2004).

[25] C. G. Salzmann, P. G. Radaelli, J. L. Finney, and E. Mayer, Phys. Chem. Chem. Phys. **10**, 6313 (2008).

[26] A. J. Leadbetter, R. C. Ward, J. W. Clark, P. A. Tucker, T. Matsuo, and H. Suga, J. Chem. Phys. **82**, 424 (1985).

[27] J. D. Jorgensen, R. A. Beyerlein, N. Watanabe, and T. G. Worlton, J. Chem. Phys. **81**, 3211 (1984).

[28] C. G. Salzmann, P. G. Radaelli, A. Hallbrucker, E. Mayer, and J. L. Finney, Science **311**, 1758 (2006).

[29] C. G. Salzmann, P. G. Radaelli, E. Mayer, and J. L. Finney, Phys. Rev. Lett. **103**, 105701 (2009).

[30] C. Knight, and S. J. Singer, J. Chem. Phys. **125**, 064506 (2006).

[31] K. Nishibata, and E. Whalley, J. Chem. Phys. **60**, 3189 (1974).

[32] B. Minceva-Sukarova, W. F. Sherman, and G. R. Wilkinson, J. Mol. Struct. **115**, 137 (1984).

[33] G. P. Arnold, R. G. Wenzel, S. W. Rabideau, N. G. Nereson, and A. L. Bowman, J. Chem. Phys. **55**, 589 (1971).

[34] C. G. Salzmann, Z. Sharif, C. L. Bull, S. T. Bramwell, A. Rosu-Finsen, and N. P. Funnell, J. Phys. Chem. C **123**, 16486 (2019).

[35] C. G. Salzmann, P. G. Radaelli, A. Hallbrucker, E. Mayer, and J. L. Finney, in *Physics and Chemistry of Ice*, edited by W. F. Kuhs (The Royal Society of Chemistry, Cambridge, 2007), pp. 521.

[36] C. G. Salzmann, B. Slater, P. G. Radaelli, J. L. Finney, J. J. Shephard, M. Rosillo-Lopez, and J. Hindley, J. Chem. Phys. **145**, 204501 (2016).

[37] A. Rosu-Finsen, and C. G. Salzmann, Chem. Sci., 515 (2019).

[38] A. Rosu-Finsen, A. Amon, J. Armstrong, F. Fernandez-Alonso, and C. G. Salzmann, J. Phys. Chem. Lett. **11**, 1106 (2020).

[39] K. Komatsu, S. Klotz, S. Machida, A. Sano-Furukawa, T. Hattori, and H. Kagi, Proc. Natl. Acad. Sci. USA **117**, 6356 (2020).

[40] C. L. Bull, N. P. Funnell, M. G. Tucker, S. Hull, D. J. Francis, and W. G. Marshall, High Pressure Res. **36**, 493 (2016).

[41] A. C. Larsen, and R. B. Von Dreele, (University of California, 1985).

[42] T. D. Kühne, M. Iannuzzi, M. Del Ben, V. V. Rybkin, P. Seewald, F. Stein, T. Laino, R. Z. Khaliullin, O. Schütt, F. Schiffmann, D. Golze, J. Wilhelm, S. Chulkov, M. H. Bani-Hashemian, V. Weber, U. Borštnik, M. Taillefumier, A. S. Jakobovits, A. Lazzaro, H. Pabst, T. Müller, R. Schade, M. Guidon, S. Andermatt, N. Holmberg, G. K. Schenter, A. Hehn, A. Bussy, F. Belleflamme, G. Tabacchi, A. Glöß, M. Lass, I.

Bethune, C. J. Mundy, C. Plessl, M. Watkins, J. VandeVondele, M. Krack, and J. Hutter, J. Chem. Phys. **152**, 194103 (2020).

[43] S. Grimme, J. Antony, S. Ehrlich, and H. Kriege, J. Chem. Phys. **132**, 154104 (2010).

[44] R. Brill, and S. Zaromb, Nature **173**, 316 (1954).

[45] L. C. Labowitz, and E. F. Westrum, J. Phys. Chem. **65**, 408 (1961).

[46] W. Ostertag, G. R. Fischer, and J. P. Williams, J. Am. Ceram. Soc. **51**, 651 (1968).

[47] K. Röttger, A. Endriss, J. Ihringer, S. Doyle, and W. F. Kuhs, Acta Cryst. **B50**, 644 (1994).

[48] A. D. Fortes, Acta Cryst. **B74**, 196 (2018).

[49] C. Lobban, J. L. Finney, and W. F. Kuhs, J. Chem. Phys. **117**, 3928 (2002).

[50] D. Londono, J. L. Finney, and W. F. Kuhs, J. Chem. Phys. **97**, 547 (1992).

[51] D. Londono, W. F. Kuhs, and J. L. Finney, Nature **332**, 141 (1988).

[52] X. Yu, J. Zhu, S. Du, H. Xu, S. C. Vogel, J. Han, T. C. Germann, J. Zhang, C. Jin, J. S. Francisco, and Y. Zhao, Proc. Natl. Acad. Sci. USA **111**, 10456 (2014).

[53] A. Y. Manakov, V. I. Voronin, A. V. Kurnosov, A. E. Teplykh, V. Y. Komarov, and Y. A. Dyadin, J. Incl. Phenom. Macro. **48**, 11 (2004).

[54] J. P. Perdew, K. Burke, and M. Ernzerhof, Phys. Rev. Lett. **77**, 3865 (1996).

[55] J. P. Perdew, K. Burke, and M. Ernzerhof, Phys. Rev. Lett. **78**, 1396 (1997).

Table 1. *Fractional atomic coordinates, fractional occupancies, order parameters and isotropic atomic-displacement parameters (U_{iso}) of D_2O $P4_12_12$ ice IX with 2.5 mol% ND_4F at 150 K and 0.300 GPa. The lattice constants are: a = 6.67255(8) Å and c = 6.80055(15) Å. Numbers in parentheses are statistical errors of the last significant digit of refined quantities. The occupancies related to the oxygen, nitrogen and fluorine atoms were calculated from the ND_4F concentration of the initial solution.*

atom label	atom type	*x*	*y*	*z*	occupancy	order parameter	U_{iso}*100
O1	O	0.1022(3)	0.3028(3)	0.2861(4)	0.9512	–	2.90(4)
O2	O	0.3908(4)	0.3908(4)	0.0000	0.9512	–	2.90(4)
D3	D	0.2181	0.3289	0.1809	0.136(1)	α	2.96(2)
D4	D	0.1344	0.3930	0.3866	0.169(1)	β	2.96(2)
D5	D	0.0188(5)	0.3337(3)	0.2145(3)	0.831(1)	$1 - \beta$	2.96(2)
D6	D	0.1152(4)	0.1624(3)	0.3035(3)	0.863(1)	$1 - \alpha$	2.96(2)
D7	D	0.3009(3)	0.3604(4)	0.1070(3)	0.864(1)	$1 - \alpha$	2.96(2)
D8	D	0.3687	0.5494	–0.0216	0.137(1)	α	2.96(2)
N1	N	0.1022(3)	0.3028(3)	0.2861(4)	0.0244	–	2.90(4)
N2	N	0.3908(4)	0.3908(4)	0.0000	0.0244	–	2.90(4)
F1	F	0.1022(3)	0.3028(3)	0.2861(4)	0.0244	–	2.90(4)
F2	F	0.3908(4)	0.3908(4)	0.0000	0.0244	–	2.90(4)